Dynamic Spatio-Temporal Data Summarization using Information Based Fusion

Humayra Tasnim[1][0000−0002−7796−7717], Soumya Dutta[2][0000−0001−5030−9979], and Melanie Moses[1]

[1] University of New Mexico, Albuquerque, New Mexico, United States
[2] Indian Institute of Technology Kanpur, Uttar Pradesh, India

Abstract. In the era of burgeoning data generation, managing large-scale datasets poses significant challenges. With the rise of computing, the volume of data produced has soared, intensifying storage and I/O overheads. To address this issue, we propose a data summarization technique that identifies informative features in key timesteps and fuses less informative ones. This approach minimizes storage requirements while preserving data features. Unlike existing methods, our method retains both raw and summarized timesteps. We utilize information-theoretic measures to devise the fusion process, visually representing underlying data patterns. We demonstrate the versatility of proposed technique across datasets from diverse application domains.

Keywords: Information Theory · Image Feature Extraction · Data Summarization · Big Data Visualization · Spatio-Temporal Data Fusion

1 Introduction

In today's data-driven world, the exponential growth in data generation has brought forth significant challenges for storage and associated I/O overheads. Modern computing capabilities have enabled the creation of massive datasets at an accelerated pace [40, 16]. Many of these datasets exhibit a dynamic temporal nature, spanning thousands of timesteps and needing large storage. Analyzing such a large number of timesteps poses significant challenges. One popular approach is to summarize the data by identifying the key timesteps. However, while key timestep-based approaches preserve the important events, automatic detection of key timesteps is non-trivial and the data dynamics for the intermediate non-key timesteps are completely ignored. Therefore, to preserve the temporal dynamics, only key timestep-based solutions may not be desired. We need novel data summarization methods that preserve both key events and overall temporal dynamics of the data in a storage-efficient compact format enabling accelerated analytics on large time-varying data.

To address the aforementioned need, we propose a data summarization technique that aims to minimize the storage overhead while preserving the salient temporal dynamics. We also emphasize visualizing these dynamics by tracking

changes over time. Our approach involves a dynamic spatio-temporal summarization (DSTS) technique, which adaptively identifies both key and redundant timesteps. We store the key timesteps and summarize redundant timesteps into a single timestep, highlighting the salient temporal characteristics of the features. The summarization technique ensures storage reduction with minimal information loss.

To achieve this, we use information-theoretic measures namely the Specific Mutual Information to guide the data fusion for the summary generation. The core idea of the summarization is to identify informative temporal features within the redundant (non-key) timesteps and fuse them using principles from information theory. By selecting the most relevant features from the redundant timesteps and summarizing through information-guided fusion, we retain the temporal dynamics. This approach optimizes storage requirements and facilitates the visualization and tracking of information change over time, providing valuable insights about data patterns.

The contributions of the paper are:

- Develop a dynamic spatio-temporal summarization (DSTS) technique for large-scale time-varying datasets. The summary provides three features: key timesteps, fused timesteps, and holistic visual representation of information change.
- Propose several information-theoretic fusion strategies and comprehensively compare, contrast, and evaluate their characteristics and applicability in summarizing the datasets.
- Demonstrate the flexibility and effectiveness of the proposed DSTS technique through application to diverse time-varying datasets including scientific flow simulations, surveillance video, and cell interactions in the immune system.
- Explore the impact of the proposed technique in optimizing data storage with minimal data loss.

2 Related Works

In this work, we focus on identifying and storing informative key timesteps while summarizing less informative (non-key) ones by fusion. Among data compression and reduction techniques, Cinema [1] is an image-based in situ data reduction and visualization approach. Lossless and lossy compression methods are also applied for data reduction [54, 13]. Among other techniques, statistical methods have been applied [58, 20, 61]. Unlike theseworks, we aim to retain information from both raw and reduced timesteps to capture information changes over time.

There are numerous approaches [64, 38, 52] that have been proposed for identifying key timesteps. These studies focus on only capturing key timesteps. Other studies focused solely on data reduction [2, 56]. Unlike these studies, our work combines summarization with key timestep selection and data reduction.

Data fusion techniques [14] for large-scale spatio-temporal datasets has been a popular field across various domains like remote sensing [32, 39],geoscience [59, 33], network architectures [29, 47], computer vision [24, 57, 60], and time-varying

scientific data [22]. In computer vision, various data summarization strategies have been explored, including Gaussian entropy fusion [25] and probabilistic skimlets fusion [62]. Additionally, deep learning methods have also been applied for summarization [63]. Unlike some existing techniques, our approach doesn't need training and can be readily applied to large-scale datasets. Moreover, it is computationally efficient, rendering it applicable for both streaming and offline data analysis.

Information theory [48, 18, 53] has been employed to measure the relationships between variables in data across multiple computational domains [36, 44, 50]. Mutual information (MI) is extensively applied for feature selection, exploration, extraction, and tracking [5, 51]. Image registration is another popular application [34, 27, 11]. MI, as well as its decomposition measures like specific mutual information and pointwise mutual information, have been widely used in multi-modal data fusion [7], data analysis, and visualization [56, 21, 28, 6, 3, 15]. Other use cases include view selection [55], feature similarity [9], and transfer function and design [43, 8].

3 Information-Driven Framework for Feature-Based Temporal Data Summaries

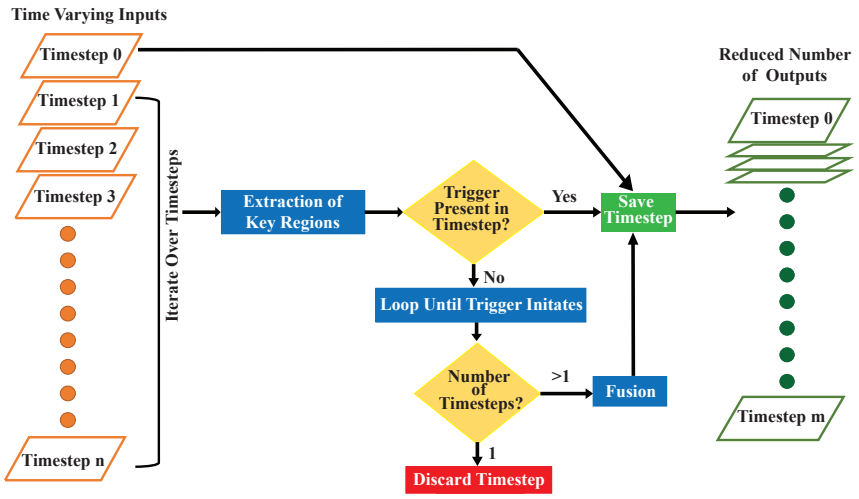

Fig. 1. Schematic diagram of our workflow. Standard computational flowchart [49] symbols are used for representations: input/output, process, decision, and arrows indicating relationships between symbols.

3.1 Framework Workflow

Figure 1 illustrates the schematic of the proposed workflow. To demonstrate each step of this workflow, we will refer to Figure 2, which serves as an illustrative application of our method using a synthetic data set. In this application, we simulate a rolling ball moving from left to right at each timestep until it exits the view area.

Our proposed method is designed for time-varying data containing various types of salient features. In Figure 2, the simulated rolling ball application consisting of 19 timesteps (T0 - T18), shows the ball's positional change over time. Each timestep is represented as 800×400 pixel 2D RGB image. At timestep T0, the frame is empty; the ball has not yet entered the view area. The ball enters at T1 and changes position until T17; finally exiting the view area at T18. The proposed method iteratively processes the sequence of input timesteps. After the first timestep, for every subsequent timesteps, the key regions are extracted using a segmentation method proposed in [31]. Criteria for extraction of such key regions is determined by the domain knowledge. In this case, the key feature is the presence of the ball and its location. So we segment the region containing the ball and create binary masked images shown in Figure 2 (masked row). These images contain only two data values: 0 (no ball) and 255 (ball).

After extracting the key region, we check if a certain property is present in that timestep. We denote this property as *trigger* which is a change in the key region. The change can be in terms of count, size, shape, connectivity, space, or association. In this rolling ball demonstration, the triggers are the first appearance and final exit of the ball from the view area. When the ball enters and then exits the area, it is considered as salient information. But the time the ball remains in the area, the only novel information is its change of position. If a trigger is present in the current timestep, then it is considered as a key timestep. Hence our method saves it as it is. If the trigger is not present, we proceed to the next timestep, do a similar check, and continue the process until a trigger is encountered. These intermediate sequential timesteps that did not have the trigger are chosen to be fused into a single timestep as the amount of novel information within such a sequence is low. If the number of timesteps to be fused is one then we can discard it as the previous timestep has the necessary information. If the number is greater than one then we perform pairwise information-guided fusion on these timesteps and convert them as one single timestep to be saved as a temporal summary. Referencing the demonstration in Figure 2, T0 is saved. Subsequently, for T1 through T17, no triggers are identified, and again, T18 is saved. Therefore, T1 through T17 are fused as shown in figure 2(a) and (b). Note that, since our method processes one timestep at a time incrementally as they appear, it can be applied to applications where data is streamed for real-time processing.

3.2 Characterization of Samplewise Information for Fusion

We use the term "sample" to refer to individual data points. Each timestep contains multiple samples representing the values of the data. In the case of

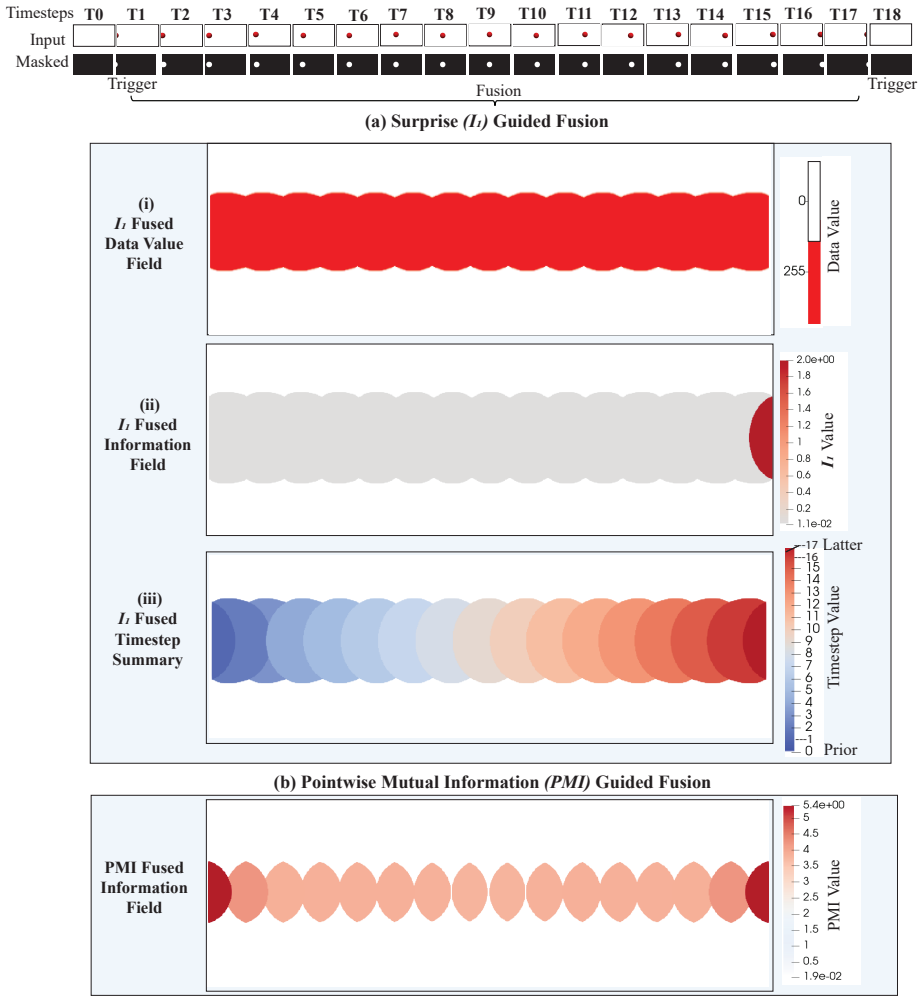

Fig. 2. Illustration using a simulated rolling ball with 19 timesteps (T0 -T18). At each timestep, the ball moves 0.5 units to the right. Timesteps are 2D RGB images with 800×400 dimensions with data (pixel) values ranging between 0 to 255 (input row). The masked row presents binary images with values 0 (no ball) and 255 (ball). T1 to T17 are fused using (a) Surprise (I_1) guided fusion and (b) PMI guided fusion. a(i) shows the I_1 fused data value field (0 white and 255 red). a(ii) shows I_1 fused information value field. a(iii) displays I_1 fused timestep summary with numbered color labels for each timestep. The numbers indicate spatial information changes over time. Surprise effectively captures spatio-temporal properties, whereas alternative PMI measure does not perform well. (b) shows the scenario with the information field using PMI values.

images like the rolling ball, these samples range from 0 to 255, while for other types of data variables, they may be scalar values. Quantifying information for these samples will help identify important spatial features for the timestep.

Mutual Inforamtion In information theory, Mutual Information (MI) [48] is a prominent measure that estimates the total amount of shared information between two random variables. Given two random variables X and Y, MI $I(X;Y)$ is formally defined as:

$$\mathrm{I}(X;Y) = \sum_{y \in Y} \sum_{x \in X} \mathrm{p}(x,y) \log \frac{\mathrm{p}(x,y)}{\mathrm{p(x)\,p(y)}} \tag{1}$$

where $\mathrm{p}(x)$ and $\mathrm{p}(y)$ are the probabilities of occurrence of values x for X and y for Y respectively. $\mathrm{p}(x,y)$ is the joint probability of occurrence of values x and y together. MI assesses the degree of association or disassociation between two random variables and gives a single value. Since we aim to extract feature-based data summaries, we need samplewise spatial and temporal information characterization. Therefore, we leverage the decomposition of MI which quantifies each data value's contribution toward the association or dissociation. The decomposition of MI is termed as Specific Mutual Information or SMI [19]. There are multiple methods for MI decomposition [19, 10]. For apprehending the fusion criteria essential for summarizing the data, the properties of the SMI measure, *Surprise* holds the most potential.

SMI Measure Surprise The Surprise measure denoted as I_1 was first introduced by [19]. Surprise quantifies the information change of the target variable after observing the individual scalar values of the reference variable. The derivation of Surprise from MI is as follows.

By definition, the conditional probability of x given y is:

$$\mathrm{p}(x|y) = \frac{\mathrm{p}(x,y)}{\mathrm{p(y)}} or\, \mathrm{p}(x,y) = \mathrm{p}(x|y)\,\mathrm{p(y)} \tag{2}$$

Replacing the joint probability in Equation 1, we get,

$$\begin{aligned} \mathrm{I}(X;Y) &= \sum_{y \in Y} \mathrm{p(y)} \sum_{\mathrm{x} \in \mathrm{X}} \mathrm{p(x|y)} \log \frac{\mathrm{p(x|y)}}{\mathrm{p(x)}} \\ &= \sum_{y \in Y} \mathrm{p(y)}\, \mathrm{I_1(y;X)} \end{aligned} \tag{3}$$

where,

$$\mathrm{I}_1(y;X) = \sum_{x \in X} \mathrm{p}(x|y) \log \frac{\mathrm{p}(x|y)}{\mathrm{p(x)}} \tag{4}$$

Equation 4 represents the surprise measure of data value y from Y after observing all the values of X. A high value for $I_1(y;X)$ means after observing y, some

previously low probable values of $x \in X$ have become highly probable. This likelihood increase is the element of surprise and a salient finding for further analysis. Surprise is also the only positive decomposition of MI since it is the Kullback-Leibler distance between p($x|y$) and p(x) [30].

3.3 Surprise (I_1) Guided Fusion Technique

When the low informative timesteps are chosen, the fusion initiates for summarization. The fusion is done on pairwise timesteps. For every pair of data samples from the timesteps, we store samples with high I_1 values. This fusion strategy was introduced by [7] for fusing different datasets to gain the most informative combination. The condition to compute the fused value using I_1-fusion is:

For every data sample pair with (x, y), the fused value, f is,

$$\mathrm{f} = \begin{cases} \mathrm{x}, & \text{if } \mathrm{I_1(x;Y)} > \mathrm{I_1(y;X)} \\ \mathrm{y}, & \text{otherwise} \end{cases} \tag{5}$$

Here x and y are individual data values from two data sets X and Y. Our fusion criteria is based on the idea of Equation 5, however, instead of different datasets we are using two subsequent timesteps from the same dataset. To fuse multiple timesteps, we begin by creating a fused timestep using the first two timesteps. Then, we repeat the fusion process by comparing the fused timestep with the next timestep and continue until all desired timesteps have been fused. Our strategy involves updating the fused timestep during each iteration and selecting the spatial and temporal values with the highest information content. By the end of the process, the resulting fused timestep will represent a summary capturing their most informative properties with direction. The fusion process is described in detail in Algorithm 1. After each fusion process, the algorithm provides 3 fused fields as shown in 2(a). I_1 fused data value field contains the values of the data samples with high surprise measure. I_1 fused information value field contains the I_1 values for the same sample positions. In the timestep summary fields, the same data samples are labeled with their originating timestep numbers.

Applying the fusion process in Algorithm 1 on T1 - T17 of the simulated rolling ball, the I_1 fused data value field is generated highlighting the path of the ball with values 255 as shown in Figure 2 a(i). The regions without the ball are valued 0. Figure 2 a(ii) represents the fused information fields with I_1 values. From the color bar's gradient, we observe that the surprise values exhibit limited variation, spanning approximately from 0 to 2. A minimal data value range results in minimal surprise variation. Figure 2 a(iii) presents the timestep summary where the numbers of originating timesteps are labeled for the salient samples. Here, we employed distinct colors to label the timesteps, enabling clear visualization and differentiation of each timestep. This color-coded representation shows the flow of information, facilitating the tracking of information changes over time. Here, the confidence threshold is employed to downplay the non-important regions. In this particular case, the threshold value is set to 255. Any value below 255, representing the absence of the ball, is assigned as timestep

0. In Figure 2 a(iii), these regions are depicted as white or transparent (steps 19 - 24 in Algorithm 1). The method reduces the number of output timesteps from 19 to 3 in the simulated rolling ball case, achieving substantial data reduction with minimal loss. The fused timestep effectively visualizes the information changes over time, serving as a summary of the original data dynamics.

3.4 Alternative Fusion Approaches

We also explore other potential information measures to devise alternative techniques for generating data summaries. These information-theoretic measures include Pointwise Mutual Information (PMI) [17], SMI measures : Predictability (I_2) [19] and *Stimulus* Specific Information (I_3) [10].

PMI Guided Fusion PMI [17] quantifies the degree of association (or disassociation) between individual data points given two variables. If X and Y are two variables, then each data point can be represented by the value pair (x, y) where $x \in X$ and $y \in Y$. The statistical association between these two points can be measured by their PMI value:

$$\mathrm{PMI}(x, y) = \log \frac{\mathrm{p}(x, y)}{\mathrm{p(x)\,p(y)}} \tag{6}$$

where $\mathrm{p}(x)$ and $\mathrm{p}(y)$ are the probabilities of occurrence of values $x \in X$ and $y \in Y$. $\mathrm{p}(x, y)$ is the joint probability of occurrence of values x and y together. Comparing Equations 1 and 6, we can infer that the expected PMI values over all occurrences of variables X and Y correspond to the MI value $I(X; Y)$. PMI is a symmetric measure that can generate values ranging from negative to positive, depending on whether the distributions are complementary or overlapping. If the information overlap is high ($\mathrm{p}(x, y) > \mathrm{p}(x)\,\mathrm{p}(y)$), then $\mathrm{PMI}(x, y) > 0$. The low association is indicated by $\mathrm{p}(x, y) < \mathrm{p}(x)\,\mathrm{p}(y)$, resulting in $\mathrm{PMI}(x, y) < 0$. If x and y are statistically independent then $\mathrm{p}(x, y) = \mathrm{p}(x)\,\mathrm{p}(y)$ and $\mathrm{PMI}(x, y) = 0$.

Given the PMI measure, we can devise a fusion strategy similar to I_1 where I_1 values are substituted with PMI values in Algorithm 1. The resulting fused information field on the simulated rolling ball is shown in Figure 2(b). We observe that PMI fails to capture the spatial characteristics of the key regions and only captures the overlapped regions indicated by high positive PMI values.

***I_2* Guided Fusion** Predictability (I_2) is another decomposition of MI introduced by [19]. This SMI measure quantifies the change in the uncertainty of one variable (X) after observing the individual value of another variable ($y \in Y$) and is computed as:

$$\mathrm{I}_2(y; X) = -\sum_{x \in X} p(x) \log p(x) + \sum_{x \in X} p(x|y) \log p(x|y) \tag{7}$$

where $y \in Y$ is the reference variable and $x \in X$ is the target variable. $\mathrm{p}(x)$ is the probabilities of occurrence of values x for X and $\mathrm{p}(x|y)$ is the conditional

Algorithm 1 Fusion Process

Input:

- data1: Array of data values from fused timestep. Initialized with the first timestep.
- data2: Array of data values from the subsequent timestep.
- Ifield1: Array of I_1 values for $I_1(x;Y)\ \forall x \in X$
- Ifield2: Array of I_1 values for $I_1(y;X)\ \forall y \in Y$
- timestep_fuse: Array of timestep values. Starts with 0
- time: Current timestep value
- conf_th: Confidence threshold for the key regions.

Output:

- fused_field_data: Array of the fused data values
- fused_field_I1: Array of the fused I_1 values
- timestep_fuse: Array of the fused timestep values.

procedure createFusionFields(*data1*, *data2*, *Ifield1*, *Ifield2*, *timestep_fuse*, *time*, *conf_th*)
  fused_field_data ← array of zeros with shape *data1*
  fused_field_I1 ← array of zeros with shape *data1*
  for $i \leftarrow 0$ to *data1.shape*[0] − 1 **do**
    for $j \leftarrow 0$ to *data1.shape*[1] − 1 **do**
      if *Ifield1*[*i*][*j*] > *Ifield2*[*i*][*j*] **then**
        fused_field_data[*i*][*j*] ← *data1*[*i*][*j*]
        fused_field_I1[*i*][*j*] ← *Ifield1*[*i*][*j*]
        if *time* = 1 **then**
          timestep_fuse[*i*][*j*] ← *time*
        end if
      else
        fused_field_data[*i*][*j*] ← *data2*[*i*][*j*]
        fused_field_I1[*i*][*j*] ← *Ifield2*[*i*][*j*]
        timestep_fuse[*i*][*j*] ← *time* + 1
      end if
    end for
  end for
  for $i \leftarrow 0$ to *data1.shape*[0] − 1 **do**
    for $j \leftarrow 0$ to *data1.shape*[1] − 1 **do**
      if *fused_field_data*[*i*][*j*] < *conf_th* **then**
        timestep_fuse[*i*][*j*] ← 0
      end if
    end for
  end for
  return *fused_field_data*, *fused_field_I1*, *timestep_fuse*
end procedure

probabilities values of x given y. In some cases, the increased uncertainty can reveal significant information about the relationship between the variables. However, when we use the I_2 measure instead of the I_1 measure in the fusion process, the resulting fused information does not offer a meaningful summary over time.

I_3 Guided Fusion Stimulus Specific Information (SSI) [10], denoted by I_3:

$$\mathrm{I}_3(y; X) = -\sum_{x \in X} p(x|y)\, \mathrm{I}_2(x; Y) \tag{8}$$

The response and stimulus are the two variables X and Y. This measure emphasizes that the most informative data values from the first variable are related to the most informative data values of the second variable [10]. In some cases, I_1 can be an alternate measure for I_3, but the interpretation is different based on the data [10]. When I_3 is used instead of I_1 on the simulated rolling ball dataset, it captured very similar properties shown in Figure 2(a). However, when applied to a more complex dataset, it failed to capture the spatial properties of the features in the summarization. This is explained in detail in Section 4.1 and shown in Figure 3(b)

4 Applications

4.1 MFIX-Exa Flow Simulation

MFIX-Exa [37] is a multiphase flow simulation developed by the National Energy Technology Laboratory (NETL), USA. Using MFIX-Exa, particle-based data is generated for studying the operational principles of chemical looping reactors. In such simulations, the formation of void regions, known as bubbles, is an important phenomenon. Understanding the temporal evolution of these bubbles holds significant importance for domain experts.

Data Context and Features For analyzing bubble dynamics, typically the raw particle data is first converted to a scalar density field. Then bubbles can be segmented as the connected regions with low particle density. For more details about this pre-processing, please refer to [23]. In this work, we assume that the scalar density fields are already available and we use 2D slices extracted from the density fields. These slices contain scalar values representing particle density. Our evaluation dataset consists of multiple timesteps (count 332), and each timestep corresponds to 2D data samples with dimensions of 488×842. The sample values fall within the range of [-1.2×10^{-6}, 29.08]. In [23], the detection, segmentation, and characterization of the bubbles are studied in an extensive manner. In our work, we use the VTK [46] library to extract the connected components and then use a low scalar density threshold value to filter the bubbles. Over time, the bubbles undergo phases like creation, merge, split, and dissolve into air. Domain experts want to comprehend the evolution

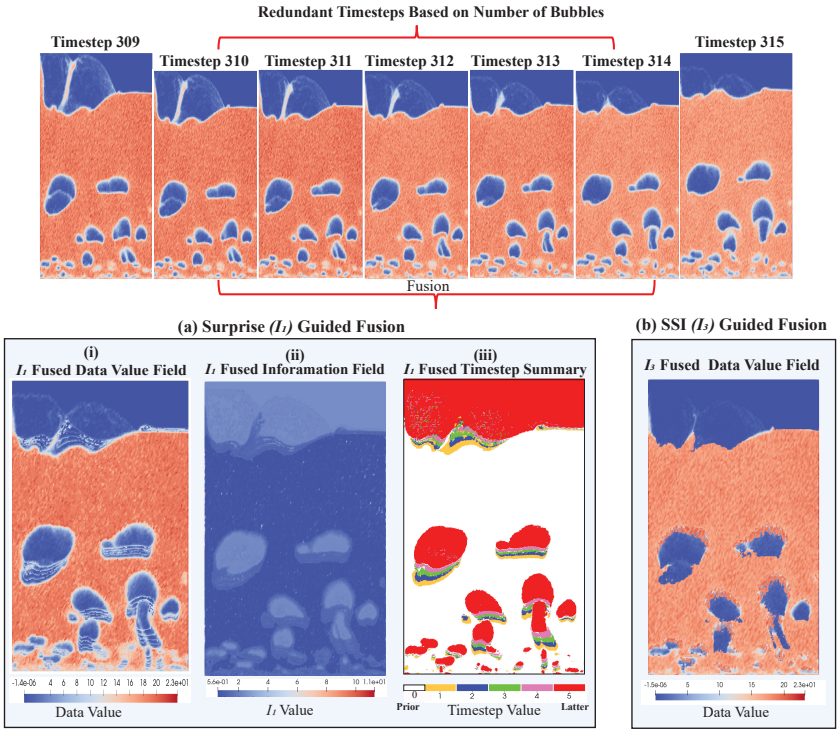

Fig. 3. Analysis of DSTS method for MFIX-Exa simulation. The first row represents a window of timesteps (309 - 315) where the bubbles are highlighted as the blue regions. Timesteps are raw images with 488×842 dimensions. 310 to 314 are fused using (a) Surprise (I_1) guided fusion (i-iii) and alternative (b) Stimulus Specific Information (SSI) or I_3 guided fusion. a(i) shows the I_1 fused data value field of the timesteps, a(ii) shows I_1 fused information value field reflecting I_1 values and a(iii) shows I_1 fused timestep summary with 5 timesteps. The color bar labels 5 different colors summarizing the direction of the bubbles in one timestep. The alternative I_3 is unable to capture the path of bubbles as reflected in (b) I_3 fused data field.

of bubbles and explore the relationships between various bubble characteristics such as their size, shape, number of bubbles, etc. [23]. Important events in this simulation can be characterized by the creation of a bubble, the merging of two or more bubbles, or the dissolving of a bubble. Note that for all of these events, the total number of bubbles will change. Hence, a timestep with the bubble number changed from a previous timestep, can be considered as a "trigger". Here, we ignore counting changes in very small bubbles since the domain experts are more concerned about the bubbles when they grow in size.

Results for Data Summarization Figure 3 shows the analysis of the DSTS method for MFIX-Exa simulation. Timesteps 309 - 315 are shown in the first row where bubbles are the blue regions. Timesteps 310 to 314, during which the number of bubbles remains unchanged, are summarized through the fusion process. Figures 3 (a) represent results from the I_1 guided fusion. The I_1 fused data value field a(i) shows the scalar values ranging $[-1.4 \times 10^{-6}, 23]$ for the fused timesteps. Here the change in bubble movement is very prominent. Figure 3 a(ii) presents the I_1 values ranging $[5.6 \times 10^{-1}, 11]$ for the fused timesteps. The range of I_1 values is smaller, making it less sensitive to bubble movement compared to particle-density values. However, it effectively highlights the main bubbles and their temporal dynamics. The timestep summary field in Figure 3 a(iii) represents the timestep values from which the bubbles originate. Here 5 timesteps are distinctly color-coded to reflect the direction of the bubbles from the start to the end position. The white background (labeled 0) filters all the density values that are of low importance for this dataset.

We have also implemented the alternative SSI (I_3) guided fusion technique as mentioned in Section 3.4 for MFIX-Exa. Figure 3(b), represents the I_3 fused data value field. Here the bubbles are only partially highlighted and the change in the bubbles' movement is also hard to interpret. While I_3 captures some spatial features of the bubbles, the edges are blurred. Thus, the *Surprise* fusion method proves to be better than the SSI measure.

4.2 Surveillance Data Analysis and Optimization

To demonstrate DSTS in security camera footage analysis, we used the publicly available SBM-RGBD Dataset [45, 12]. This dataset was originally created for the Workshop on Background Learning for Detection and Tracking from RGBD Videos [41]. The dataset comprises 33 RGBD videos, totaling 15033 timesteps, recorded indoors using a Microsoft Kinect sensor [12]. The dataset contains videos capturing moving objects at intervals, which aligns with our data requirements. Here, we used one of the videos that shows four individuals walking in and out of the view area, engaging in discussions, and writing on a whiteboard. The most significant impact of our proposed method in this application is on archiving the storage optimization.

Data Context and features The videos have 640×480 resolution and the length is 1400 timesteps. The key regions (features) are the individuals and

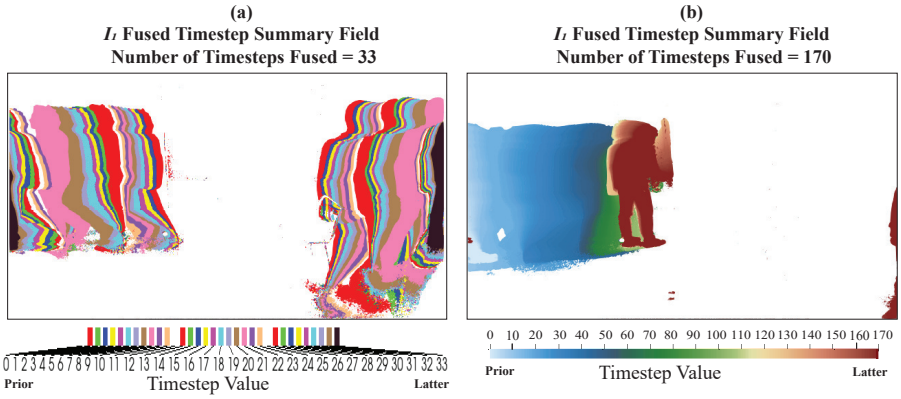

Fig. 4. Results of the DSTS method for SBM-RGBD dataset. Here the emphasis is on representing the extensive number of timestep summaries. (a) shows a summarization of 33 fused timesteps using a discrete color bar. (b) showcases a summarization of 170 fused timesteps, employing a continuous color bar to depict information changes over a longer period. The color bars point out the spatial direction of the information flow by denoting the prior and latter states.

their movement. The whiteboard and a chair are stationary in the background. To extract key regions, we have used a background subtraction algorithm, called ViBe [4]. The algorithm aims to identify moving objects within consecutive images or videos by distinguishing between the foreground (moving objects) and the background (stationary elements). The ViBe algorithm is adaptive and computationally lightweight, making it suitable for real-time applications. Its straightforward pseudocode in [4] facilitates easy implementation. The ViBe algorithm converts the RGB images into masked binary images with segmented individuals.

In scenarios with multiple individuals, we adopt a concept similar to that used for counting bubbles in the MFIX-Exa (Section 4.1). We apply the concept to count the number of individuals in each timestep by analyzing the largest connected regions in the masked images. Since it is a binary image, the data samples have two values: 0 (no individual) and 255 (individual). By setting a size threshold, we can accurately count the number of individuals in each timestep. Given that individuals move in and out of the view area, the number of individuals can be used as a trigger for our application. Whenever a person enters or exits, that is a key timestep. The consecutive timesteps between two triggers are then fused using Algorithm 1. This fusion process effectively summarizes the movement patterns of individuals within one timestep.

Results for Data Summarization In Figure 4(a), the summarization field depicts a fusion of 33 timesteps, where two individuals walk out of the view area. The leftmost person exits first, initiating the trigger and stopping the fusion process. Each timestep is represented by a discrete color, highlighting the

changes in movement over 33 timesteps. Sample values below 255 are set to 0, representing the white background, as the data value of individuals is 255. Figure 4(b) shows a timestep summary for a longer period of 170 timesteps. The summarization field captures an individual walking into the view area and writing on the board, while another person has just stepped in, initiating the trigger. Continuous colors are used to display the movement changes.Expectedly, key and summarized timesteps in this dataset result in a significant reduction from 1400 timesteps to only 49 timesteps. The highest number of timesteps being fused is 262.

4.3 Tracking Cell Interactions in Lymph Nodes

This dataset contains consecutive images of cellular interactions within the lymph node (LN). LNs are essential for immune function, playing a crucial role in initiating immune response and facilitating immune cell communication [35]. We reanalyze data from [50], where information theory-based approaches were used to identify and quantify the spatial relationships between naïve T cells and other cell types like Dendritic Cells (DCs). The data for the study was gathered using two-photon microscopy (2PM) [42] to acquire 3D image stacks of LN tissue samples from mice. The imaging process captured dynamic movies lasting 10 to 45 minutes, resulting in a sequence of 3D images. This dataset is well-suited for the application of our method.

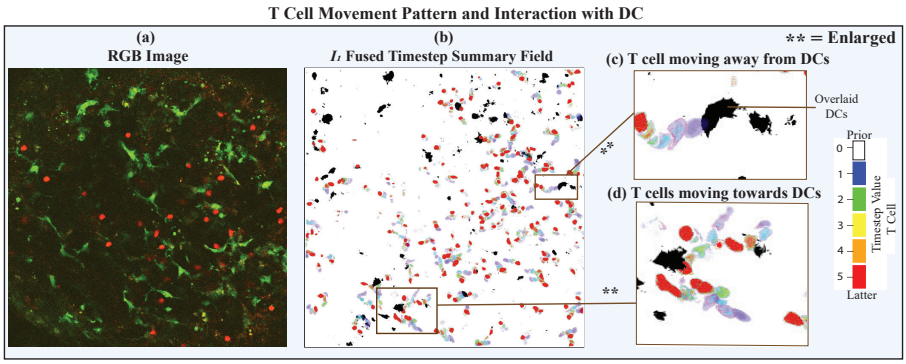

Fig. 5. Results of the DSTS method for cell interaction in Lymph Node. The results emphasize T cell movement patterns and interaction with DCs in LN. (a) is an illustrative timestep from the dataset. Here red indicates the T cells and green indicates the DCs. (b) is the surprise fused timestep summary fields of T cell for 5 timesteps. The black cells in the field are overlaid DCs to highlight cell contact. (c) and (d) are 2 enlarged positions from the (b) field to emphasize T cell movement. (c) shows that a T cell is moving away from the DCs. (d) shows multiple T cells moving toward the DCs. The corresponding timestep values are provided in the color bars to highlight the direction.

Data Context and Features Figure 5(a) shows an RGB image with T cells dyed red and Dendritic Cells (DC) dyed green. Each voxel contains the color intensities of the dye in the red, blue, and green channels. For every time step, we extract the red and green channels into two separate images. We focus on the red channel in order to analyze T-cell motility. Because these images contain a lot of noise, we implement a pre-processing step using the median filter [26], to reduce noise while preserving the edges of the cells for improved visualization. Since the red channels specifically represent the T cells, no segmentation is required. In [50], MI and normalized mutual information (NMI) were used to quantify associations between cells. Here, we use the MI value between two cell types as a "trigger". If the MI value for a specific timestep exceeds a specified threshold, we save that as a key timestep. If the MI value falls below the threshold, we find the next timestep in which the MI value exceeds the trigger threshold and fuse the intermediate ones.

Results of Data Summarization Figure 5 focuses on the T cell movement and interaction with DCs in the summarized timesteps. Figure 5(a) is a sample timestep of the T:DC dataset with $512 \times 512 \times 22$ dimensions. This dataset has a total of 51 timesteps. Figure 5(b) displays the I_1 fused timestep summary field, representing five fused timesteps from this dataset. The black cells in the summarization represent the DCs' value field overlaid on the fused summary field, visually illustrating the physical interactions between T cells and DCs. Given that there are multiple interactions captured in each timestep, we highlight two specific interactions by enlarging the locations in Figures 5(c) and (d). In Figure 5(c), we observe a T cell moving away from the DCs. The color bar on the right indicates the first (blue) and last (red) timesteps in the summary field, clearly indicating the movement direction. In Figure 5(d), we see multiple T cells moving toward the DCs making explicit contact. This visualization allows for a comprehensive understanding of the dynamic interactions between T cells and DCs, providing valuable insights into the temporal dynamics of immune cell communication.

5 Discussion

The proposed DSTS technique has demonstrated its effectiveness and flexibility across several applications. Starting with a synthetic simulation of a rolling ball to analyzing complex cellular interactions within lymph nodes, the method effectively showcased its robustness. The combination of the key and fused timestep resulting from the method provides a compact yet comprehensive data summarization.

We select applications from multiple domains to shed light on different aspects of the DSTS method. This technique offers a practical solution to downsize and analyze the features in the MFIX-Exa simulation. This application analysis establishes that the method can handle raw scalar data as well as image-based data that incorporates the rest of the applications. The RGBD tracking dataset

is introduced to show the method's ability to summarize and highlight important movement patterns of individuals in a video sequence. The results from this dataset reflect that longer fused timesteps are equally apprehensible as the shorter ones. This has promising implications for surveillance and security applications. The cellular interaction in LN is a more complex dataset. T cells which are the key regions (features) are ample in number and the interactions with DCs are sporadic in nature. Our method is able to track multiple cell interactions. The summarization highlights immune cell communication by providing a comprehensive visualization of the T cell movement. This visualization potentially introduces new possibilities for immunological research.

All the applications in this work present post hoc data analysis. Since the method is not computationally expensive it can be easily combined to analyzing data in a streaming framework. Through the integration of this method in any in situ streaming framework, the resulting data will be summarized in real-time ensuring optimal storage reduction.

We acknowledge that challenges may arise in selecting appropriate triggers and threshold values, especially in complex datasets with multiple key features, interactions, and noise. However, the flexibility of the technique allows for the adjustment of parameters to tailor the summarization process to different applications. Additionally, future research could explore combining different information-theoretic measures to further enhance the summarization capabilities to multivariate time-varying datasets.

Data Availability

All the code and data are available at https://github.com/htasnim/Dynamic-Spatio-Temporal-Data-Summarization

Acknowledgments. We thank Professor Judy Cannon (UNM) for providing the biological data, and Dr. Matthew Fricke (UNM) for discussions on cell analysis.

Disclosure of Interests. The authors declare that they have no known competing financial interests or personal relationships that could have appeared to influence the work reported in this paper.

References

1. Ahrens, J., Jourdain, S., O'Leary, P., Patchett, J., Rogers, D.H., Petersen, M.: An Image-Based Approach to Extreme Scale in Situ Visualization and Analysis. International Conference for High Performance Computing, Networking, Storage and Analysis, SC **2015-January**, 424–434 (2014). https://doi.org/10.1109/SC.2014.40
2. Akiba, H., Fout, N., Ma, K.L.: Simultaneous classification of time-varying volume data based on the time histogram. In: EuroVis. vol. 6, pp. 1–8 (2006)
3. Akiba, H., Ma, K.L., Chen, J.H., Hawkes, E.R.: Visualizing multivariate volume data from turbulent combustion simulations. Computing in Science and Engineering **9**(2), 76–83 (2007). https://doi.org/10.1109/MCSE.2007.42

4. Barnich, O., Van Droogenbroeck, M.: Vibe: A universal background subtraction algorithm for video sequences. IEEE Transactions on Image processing **20**(6), 1709–1724 (2010)
5. Biswas, A., Dutta, S., Shen, H.W., Woodring, J.: An information-aware framework for exploring multivariate data sets. IEEE Transactions on Visualization and Computer Graphics **19**, 2683–2692 (2013). https://doi.org/10.1109/TVCG.2013.133
6. Bramon, R., Ruiz, M., Bardera, A., Boada, I., Feixas, M., Sbert, M.: An information-theoretic observation channel for volume visualization. Computer Graphics Forum **32**(3 PART4), 411–420 (2013). https://doi.org/10.1111/cgf.12128
7. Bramon, R., Boada, I., Bardera, A., Rodríguez, J., Feixas, M., Puig, J., Sbert, M.: Multimodal data fusion based on mutual information. IEEE Transactions on Visualization and Computer Graphics **18**(9), 1574–1587 (2012). https://doi.org/10.1109/TVCG.2011.280
8. Bramon, R., Ruiz, M., Bardera, A., Boada, I., Feixas, M., Sbert, M.: Information theory-based automatic multimodal transfer function design. IEEE Journal of Biomedical and Health Informatics **17**(4), 870–880 (2013). https://doi.org/10.1109/JBHI.2013.2263227
9. Bruckner, S., Möller, T.: Isosurface similarity maps. In: Computer Graphics Forum. vol. 29, pp. 773–782. Wiley Online Library (2010)
10. Butts, D.A.: How much information is associated with a particular stimulus? Network: Computation in Neural Systems **14**(2), 177–187 (2003). https://doi.org/10.1088/0954-898X_14_2_301
11. Cahill, N.D.: Normalized measures of mutual information with general definitions of entropy for multimodal image registration. Lecture Notes in Computer Science (including subseries Lecture Notes in Artificial Intelligence and Lecture Notes in Bioinformatics) **6204 LNCS**(8), 258–268 (2010). https://doi.org/10.1007/978-3-642-14366-3_23
12. Camplani, M., Maddalena, L., Moyá Alcover, G., Petrosino, A., Salgado, L.: A Benchmarking Framework for Background Subtraction in RGBD Videos. Lecture Notes in Computer Science (including subseries Lecture Notes in Artificial Intelligence and Lecture Notes in Bioinformatics) **10590 LNCS**, 219–229 (2017). https://doi.org/10.1007/978-3-319-70742-6_21
13. Cappello, F., Di, S., Li, S., Liang, X., Gok, A.M., Tao, D., Yoon, C.H., Wu, X.C., Alexeev, Y., Chong, F.T.: Use cases of lossy compression for floating-point data in scientific data sets. The International Journal of High Performance Computing Applications **33**(6), 1201–1220 (2019)
14. Castanedo, F., et al.: A review of data fusion techniques. The scientific world journal **2013** (2013)
15. Chen, M., Feixas, M., Viola, I., Bardera, A., Shen, H.W., Sbert, M.: Information theory tools for visualization. CRC Press (2016)
16. Childs, H.: Data exploration at the exascale. Supercomputing frontiers and innovations **2**(3), 5–13 (2015)
17. Church, K., Hanks, P.: Word association norms, mutual information, and lexicography. Computational linguistics **16**(1), 22–29 (1990)
18. Cover, T.M., Thomas, J.A.: Elements of Information Theory 2nd Edition (Wiley Series in Telecommunications and Signal Processing). Wiley-Interscience (July 2006)
19. DeWeese, M.R., Meister, M.: How to measure the information gained from one symbol. Network: Computation in Neural Systems (1999). https://doi.org/10.1088/0954-898X_10_4_303

20. Dutta, S., Chen, C.M., Heinlein, G., Shen, H.W., Chen, J.P.: In situ distribution guided analysis and visualization of transonic jet engine simulations. IEEE transactions on visualization and computer graphics **23**(1), 811–820 (2016)
21. Dutta, S., Liu, X., Biswas, A., Shen, H.W., Chen, J.P.: Pointwise information guided visual analysis of time-varying multi-fields. SIGGRAPH Asia 2017 Symposium on Visualization, SA 2017 (2017). https://doi.org/10.1145/3139295.3139298
22. Dutta, S., Tasnim, H., Turton, T.L., Ahrens, J.: In Situ Adaptive Spatio-Temporal Data Summarization. Proceedings - 2021 IEEE International Conference on Big Data, Big Data 2021 pp. 315–321 (2021). https://doi.org/10.1109/BigData52589.2021.9671581
23. Dutta, S., Turton, T., Rogers, D., Musser, J.M., Ahrens, J., Almgren, A.S.: In situ feature analysis for large-scale multiphase flow simulations. Journal of Computational Science **63**(July), 101773 (2022). https://doi.org/10.1016/j.jocs.2022.101773, https://doi.org/10.1016/j.jocs.2022.101773
24. Duzceker, A., Galliani, S., Vogel, C., Speciale, P., Dusmanu, M., Pollefeys, M.: Deepvideomvs: Multi-view stereo on video with recurrent spatio-temporal fusion. In: Proceedings of the IEEE/CVF Conference on Computer Vision and Pattern Recognition. pp. 15324–15333 (2021)
25. Fu, Y., Guo, Y., Zhu, Y., Liu, F., Song, C., Zhou, Z.H.: Multi-view video summarization. IEEE Transactions on Multimedia **12**(7), 717–729 (2010)
26. Gonzales, R.C., Wintz, P.: Digital image processing. Addison-Wesley Longman Publishing Co., Inc. (1987)
27. Hill, D.L., Batchelor, P.G., Holden, M., Hawkes, D.J.: Medical image registration. Physics in medicine & biology **46**(3), R1 (2001)
28. Isola, P., Zoran, D., Krishnan, D., Adelson, E.H.: Crisp boundary detection using pointwise mutual information. Lecture Notes in Computer Science (including subseries Lecture Notes in Artificial Intelligence and Lecture Notes in Bioinformatics) **8691 LNCS**(PART 3), 799–814 (2014). https://doi.org/10.1007/978-3-319-10578-9_52
29. Kashinath, S.A., Mostafa, S.A., Mustapha, A., Mahdin, H., Lim, D., Mahmoud, M.A., Mohammed, M.A., Al-Rimy, B.A.S., Fudzee, M.F.M., Yang, T.J.: Review of data fusion methods for real-time and multi-sensor traffic flow analysis. IEEE Access **9**, 51258–51276 (2021)
30. Kullback, S., Leibler, R.A.: On information and sufficiency. The annals of mathematical statistics **22**(1), 79–86 (1951)
31. Kuruvilla, J., Sukumaran, D., Sankar, A., Joy, S.P.: A review on image processing and image segmentation. In: 2016 International Conference on Data Mining and Advanced Computing (SAPIENCE). pp. 198–203 (2016). https://doi.org/10.1109/SAPIENCE.2016.7684170
32. Li, J., Li, Y., He, L., Chen, J., Plaza, A.: Spatio-temporal fusion for remote sensing data: An overview and new benchmark. Science China Information Sciences **63**, 1–17 (2020)
33. Ma, P., Kang, E.L.: Spatio-temporal data fusion for massive sea surface temperature data from modis and amsr-e instruments. Environmetrics **31**(2), e2594 (2020)
34. Maes, F., Collignon, A., Vandermeulen, D., Marchal, G., Suetens, P.: Multimodality image registration by maximization of mutual information. IEEE Transactions on Medical Imaging **16**(2), 187–198 (1997)
35. Mirsky, H.P., Miller, M.J., Linderman, J.J., Kirschner, D.E.: Systems biology approaches for understanding cellular mechanisms of immunity in lymph nodes during infection. Journal of theoretical biology **287**, 160–170 (2011)

36. Moore, D.G., Valentini, G., Walker, S.I., Levin, M.: Inform: Efficient information-theoretic analysis of collective behaviors. Frontiers Robotics AI **5**(JUN), 1–14 (2018). https://doi.org/10.3389/frobt.2018.00060
37. Musser, J., Almgren, A.S., Fullmer, W.D., Antepara, O., Bell, J.B., Blaschke, J., Gott, K., Myers, A., Porcu, R., Rangarajan, D., Rosso, M., Zhang, W., Syamlal, M.: MFIX-Exa: A path toward exascale CFD-DEM simulations. International Journal of High Performance Computing Applications **36**(1), 40–58 (2022). https://doi.org/10.1177/10943420211009293
38. Myers, K., Lawrence, E., Fugate, M., Bowen, C.M., Ticknor, L., Woodring, J., Wendelberger, J., Ahrens, J.: Partitioning a large simulation as it runs. Technometrics **58**(3), 329–340 (2016)
39. Nguyen, H., Katzfuss, M., Cressie, N., Braverman, A.: Spatio-temporal data fusion for very large remote sensing datasets. Technometrics **56**(2), 174–185 (2014)
40. Reed, D.A., Dongarra, J.: Exascale computing and big data. Communications of the ACM **58**(7), 56–68 (2015)
41. Background learning for detection and tracking from rgbd videos. https://rgbd2017.na.icar.cnr.it/, accessed: 2023-09-22
42. Rubart, M.: Two-photon microscopy of cells and tissue. Circulation research **95**(12), 1154–1166 (2004)
43. Ruiz, M., Bardera, A., Boada, I., Viola, I., Feixas, M., Sbert, M.: Automatic transfer functions based on informational divergence. IEEE Transactions on Visualization and Computer Graphics **17**(12), 1932–1941 (2011). https://doi.org/10.1109/TVCG.2011.173
44. Sbert, M., Feixas, M., Rigau, J., Chover, M., Viola, I.: Information theory tools for computer graphics. Springer Nature (2022)
45. Sbm-rgbd dataset. https://rgbd2017.na.icar.cnr.it/SBM-RGBDdataset.html, accessed: 2023-09-22
46. Schroeder, W., Martin, K.M., Lorensen, W.E.: The visualization toolkit an object-oriented approach to 3D graphics. Prentice-Hall, Inc. (1998)
47. Shah, Z., Anwar, A., Mahmood, A.N., Tari, Z., Zomaya, A.Y.: A spatiotemporal data summarization approach for real-time operation of smart grid. IEEE Transactions on Big Data **6**(4), 624–637 (2017)
48. Shannon, C.E.: A Mathematical Theory of Communication. Bell System Technical Journal **27**(3), 379–423 (1948). https://doi.org/10.1002/j.1538-7305.1948.tb01338.x
49. Sipser, M.: Introduction to the Theory of Computation. Course Technology, Boston, MA, third edn. (2013)
50. Tasnim, H., Fricke, G., Byrum, J., Sotiris, J., Cannon, J., Moses, M.: Quantitative measurement of naïve T cell association with dendritic cells, FRCs, and blood vessels in lymph nodes. Frontiers in Immunology **9**(JUL) (2018). https://doi.org/10.3389/fimmu.2018.01571
51. Tasnim, H., Dutta, S., Turton, T.L., Rogers, D.H., Moses, M.E.: Information-Theoretic Exploration of Multivariate Time-Varying Image Databases. Computing in Science and Engineering **24**(3), 61–70 (2022). https://doi.org/10.1109/MCSE.2022.3188291
52. Tong, X., Lee, T.Y., Shen, H.W.: Salient time steps selection from large scale time-varying data sets with dynamic time warping. In: IEEE symposium on large data analysis and visualization (LDAV). pp. 49–56. IEEE (2012)
53. Verdu, S.: Fifty years of shannon theory. IEEE Transactions on Information Theory **44**(6), 2057–2078 (1998). https://doi.org/10.1109/18.720531

54. Vidhya, K., Karthikeyan, G., Divakar, P., Ezhumalai, S.: A review of lossless and lossy image compression techniques. Int. Res. J. Eng. Technol.(IRJET) **3**(4), 616–7 (2016)
55. Viola, I., Feixas, M., Sbert, M., Groller, M.E.: Importance-driven focus of attention. IEEE transactions on visualization and computer graphics **12**(5), 933–940 (2006)
56. Wang, C., Yu, H., Ma, K.L.: Importance-driven time-varying data visualization. IEEE Transactions on Visualization and Computer Graphics **14**(6), 1547–1554 (2008)
57. Wang, Q., Tang, Y., Tong, X., Atkinson, P.M.: Virtual image pair-based spatio-temporal fusion. Remote Sensing of Environment **249**, 112009 (2020)
58. Woodring, J., Ahrens, J., Figg, J., Wendelberger, J., Habib, S., Heitmann, K.: In-situ sampling of a large-scale particle simulation for interactive visualization and analysis. In: Computer Graphics Forum. vol. 30, pp. 1151–1160. Wiley Online Library (2011)
59. Wu, P., Yin, Z., Zeng, C., Duan, S.B., Göttsche, F.M., Ma, X., Li, X., Yang, H., Shen, H.: Spatially continuous and high-resolution land surface temperature product generation: A review of reconstruction and spatiotemporal fusion techniques. IEEE Geoscience and Remote Sensing Magazine **9**(3), 112–137 (2021)
60. Xue, J., Leung, Y., Fung, T.: A bayesian data fusion approach to spatio-temporal fusion of remotely sensed images. Remote Sensing **9**(12), 1310 (2017)
61. Ye, Y.C., Neuroth, T., Sauer, F., Ma, K.L., Borghesi, G., Konduri, A., Kolla, H., Chen, J.: In situ generated probability distribution functions for interactive post hoc visualization and analysis. In: 2016 IEEE 6th Symposium on Large Data Analysis and Visualization (LDAV). pp. 65–74. IEEE (2016)
62. Zhang, L., Gao, Y., Hong, R., Hu, Y., Ji, R., Dai, Q.: Probabilistic skimlets fusion for summarizing multiple consumer landmark videos. IEEE Transactions on Multimedia **17**(1), 40–49 (2014)
63. Zhong, S.h., Wu, J., Jiang, J.: Video summarization via spatio-temporal deep architecture. Neurocomputing **332**, 224–235 (2019)
64. Zhou, B., Chiang, Y.J.: Key time steps selection for large-scale time-varying volume datasets using an information-theoretic storyboard. In: Computer Graphics Forum. vol. 37, pp. 37–49. Wiley Online Library (2018)